The object of this study is the wear resistance of surfaces after electric spark alloying in contact with elastically fixed abrasive grains. The task addressed relates to the lack of technological modes for electric spark processing, in particular for hard alloys T15K6 and VK8. A rational mode has been determined, under which samples with an optimal surface profile, a uniform structure, and minimal internal defects were obtained.

The choice of the technique for machining high-wear surfaces by the electric spark alloying method is due to its simplicity and accessibility.

Waste can be used as electrodes, specifically hard alloy plates of a cutting tool that have failed. At the same time, there are a number of unresolved issues related to the choice of optimal machining modes that would ensure high wear resistance of the machined surfaces.

A technique for testing machined parts for wear has been proposed. It was found that the highest predicted wear resistance would be demonstrated by parts processed by the electric spark alloying (ESA) method using the VK8 electrode, with the capacitor bank capacity of 330 ± 30 μF and the electrode vibration frequency of 125 ± 25 Hz. They combine high surface microhardness (13.5 MPa) and residual compressive stresses in the deposited layer (–90 MPa).

The results are attributed to the physical and mechanical processes occurring in the metal during electric spark alloying. These conditions were created by different values of technological parameters. A feature of the results is that it was established that not only the hardness of the deposited layer but also the magnitude of internal stresses in this layer have a significant impact on the operational parameters.

Practical application implies that electric spark alloying could become an alternative technology for strengthening the surfaces of parts that work in contact with abrasives (mechanical engineering, medicine)

Keywords: electric spark alloying, hard alloys, tribological studies, spectral analysis, microhardness, wear

UDC 621.9.048:621.92
DOI: 10.15587/1729-4061.2025.331878

DETERMINING THE RATIONAL TECHNOLOGICAL PROCESSING MODES FOR ACHIEVING OPTIMAL OPERATIONAL CHARACTERISTICS OF THE SURFACE LAYER OBTAINED BY ELECTRIC SPARK ALLOYING USING CARBIDE ELECTRODES

Ihor Prunko
Corresponding author
PhD, Associate Professor*
E-mail: ihor.prunko@nung.edu.ua
Tetyana Voytsehivska*
Yaroslav Dem'yanchuk
PhD, Associate Professor
Department of Construction and Civil Engineering**
*Department of Motor Vehicle Transport**
**Ivano-Frankivsk National Technical University of Oil and Gas
Karpatska str., 15, Ivano-Frankivsk, Ukraine, 76019

Received 20.03.2025
Received in revised form 26.05.2025
Accepted date 12.06.2025
Published date 25.06.2025

How to Cite: *Prunko, I., Voytsehivska, T., Dem'yanchuk, Y. (2025). Determining the rational technological processing modes for achieving optimal operational characteristics of the surface layer obtained by electric spark alloying using carbide electrodes. Eastern-European Journal of Enterprise Technologies, 3 (12 (135)), 28–37. https://doi.org/10.15587/1729-4061.2025.331878*

1. Introduction

One of the main directions in the development of production and operation of various technological equipment is to improve its qualitative and economic indicators. Increasing durability of operation of machines and mechanisms makes it possible not only to significantly improve labor productivity but also release significant resources of labor force, to achieve economy of raw materials and energy carriers, which is especially relevant under the conditions of current Ukrainian economy.

One area to increase the wear resistance of working surfaces is application of wear-resistant coatings by method of electric spark alloying (ESA). This technique is widely used to improve operating characteristics (hardness, wear resistance) of parts operating under conditions of high friction loads – rolls of rolling mills, dies, teeth of excavator buckets, etc. A positive feature of this technique is the possibility of using it both in manufacturing of new parts, and in restoring their dimensional and operational characteristics in the process of restoration.

However, despite its prospects, the ESA method is practically not used for wear-resistant parts in the oil and gas industry in general and hydraulic pump rods, in particular.

Applying a wear-resistant coating by the method of electric spark alloying is advantageously different from other technologies for applying wear-resistant coatings in that it makes it possible to obtain surfaces with predetermined physical and operational properties. Coatings obtained by ESA are characterized by high hardness, wear resistance, high coefficient of adhesion of the applied material to the substrate material, the ability to work under conditions of alternating loads without peeling of the coating.

However, the widespread introduction of wear-resistant coatings obtained by ESA is hindered by the lack of scientifically based recommendations regarding the optimal choice of wear-resistant materials, their areas of application, optimal technologies, and application modes.

Based on the above, improving the durability and wear resistance of hydraulic pump rods using the ESA method is a relevant task that requires more in-depth study.

2. Literature review and problem statement

In [1], the results of the study on the mass transfer process carried out during the formation of a surface layer by the ESA method on samples of steel 45 are reported. The authors consider the application of multicomponent coatings, where indium, tin, and copper were used as soft antifriction metals, and tungsten and a hard alloy of the VK8 brand were used as wear-resistant materials. A mathematical model for calculating the main technological parameters of ESA is given, which makes it possible to predict the increase in mass and the increase in size on the cathode (part). However, issues related directly to tribological studies of the applied layers remain unresolved. The likely reason is associated with the large volume of research work, which does not correspond to the profile of the cited paper.

An option for overcoming this challenge is the approach proposed in [2]. The authors investigated the mechanical and tribological properties of Hardox 400 steel after electric spark alloying (ESA) using electrodes made of T15K6, BK6 hard alloy carbides. Iron-based composite materials such as 12S2 and WSi_2 (76.6% W; 23.4% Si) were also used as electrodes. The energy parameters (energy of pulse discharges, their amplitude and repetition rate) and technological parameters (type of movement of the processed electrode, vibration, or vibration/rotation) were optimized. The electrode composition was also proposed, under which the highest quality surface layers with high wear resistance are observed. However, the authors explain the increase in wear resistance of the obtained coatings solely by the increase in the hardness of the applied surfaces, without taking into account the influence of structural changes in the applied layer.

Work [3] considers the analysis of mechanism for thermal spraying, electric spark doping technology, and magnetron sputtering, comparing the advantages and disadvantages of each method, and also focusing on the influence of compositions, process parameters, and the subsequent treatment process on the microstructure and properties of the coating. Since the authors pay attention to the analysis of processes as a whole, the work does not consider specific examples of tasks related to ESA.

The authors of work [4] consider the strengthening process using different electrode materials. The study of coating materials is mainly focused on hard alloy and ceramic materials, the combination of other technologies with the technology of electric spark deposition, and the development of composite processing. Despite the thoroughly conducted metallographic studies, it was not intended to conduct parallel tribological studies to confirm the conclusions obtained. The reason for this may be the cost of such studies in terms of the cost and duration.

In [5], based on the state of research on ESA of titanium alloys, the influence of ESA technology on corrosion resistance, oxidation resistance at high temperatures, and biocompatibility of titanium alloys is considered in detail. The issues raised in the work relate more to medical issues. They can be applied to a lesser extent to mechanism components.

In work [6], the application of layers using different process parameters was considered. The heat supply was changed at three levels. The resulting microstructure was analyzed using optical and scanning electron microscopy. The layer was characterized by overlapping layers with a mixed microstructure. The average hardness did not depend on the process parameters. Both porosity within the layers and cracks at the interface between the layer and the substrate were detected. Porosity decreased with increasing heat input and increased the average crack length. However, the authors did not consider the influence of process parameters on the size of defects. Further research may focus on reducing defects, for example, using automated coating.

The authors of [7] consider the application of Cr-coating on M50 steel by the method of electric spark deposition with different parameters. The influence of deposition parameters on the microstructure and corrosion behavior of coatings was experimentally investigated. The authors claim that local corrosion occurs in the coating when there are through cracks. The coating applied at 150 V, 60 μF, has the minimum defect density and the best anti-corrosion behavior. However, the work does not consider the causes of these cracks and their influence on the wear resistance of hardened surfaces.

The authors of [8] claim that cracking of the coating at low spark energy differs from cracking at high spark energy. In addition, it was found that with increasing spark energy, the hardness and thickness of the coating increase. It is also shown that the process parameters have a mutual influence on the characteristics of the coating, and there is an optimal condition for achieving a strong coating. The maximum hardness of the coating was obtained at high spark energies. However, the authors do not consider the influence of these defects on the wear resistance of the coatings.

The authors of work [9] consider the process of sulfur saturation (sulfidation) of steel 20 and malleable iron surfaces by the ESA method using a special electrode-tool made of stainless steel 12X18N10T. Thorough metallographic studies and elemental analysis presented in this work do not provide an answer to the question of the influence of processing modes on the structure and performance characteristics of the resulting layer.

The authors of [10] claim that TiC and WC coatings demonstrate a sharp increase in microhardness, up to 5 times. The WC coating improved wear resistance by more than 5 times, while the TiC and Mo coatings also improved it by approximately 2.5 times. Electrochemical tests were carried out to study the corrosion resistance of the coatings. The Mo coating demonstrated a significant improvement in corrosion resistance in 5% NaCl solutions, corroding 350 times slower than stainless steel. However, as in most previous works, the authors emphasize that the increase in wear resistance occurs solely due to an increase in the hardness of the deposited layer. The effect of microdefects is not taken into account.

In general, it can be concluded that the reviewed literature [1–10] does not specify requirements for the structure and properties of electrode materials. This prevents raising the issue of industrial production of electrode materials for surface hardening by electric spark alloying. So far, standard hard alloys, such as TC and VK, are used for these purposes.

All this leads to insufficiently effective hardening of the treated surfaces and unjustified consumption of scarce hard alloys and does not make it possible to fully implement the high physical and mechanical properties of tungsten carbide. In this regard, it is advisable to conduct a study aimed at determining the patterns of erosion and the formation of a hardened layer depending on the composition and structure of the electrode material and processing modes. The data obtained are necessary for devising principles for designing

electrode materials that make it possible to form highly effective coatings.

In addition, it is necessary to apply a technique of wear testing that would allow the most accurate modeling of the process of contact of the hardened surface with elastically fixed abrasive grains. This phenomenon often occurs when rods of various purposes come into contact with a seal.

Although the reviewed literature contains references to the influence of internal stresses in the surface layer on the performance of hardened parts, they are not specified.

3. The aim and objectives of the study

The purpose of our study is to find rational technological modes for strengthening parts by electric spark alloying using hard alloy electrodes, which will ensure maximum wear resistance of the treated surfaces.

To achieve the goal, the following tasks are set:

– to conduct a study on the applied layers using metallographic microscopy;

– to determine residual stresses in the applied coatings;

– to conduct tribological studies of the strengthened surfaces.

4. The study materials and methods

4. 1. The object and hypothesis of the study

The object of our study is the wear resistance of surfaces after electric spark alloying in contact with elastically fixed abrasive grains. This type of wear is observed in contact, in particular, with hydraulic cylinder rods, shafts with seals, under which abrasive grains have fallen.

The hypothesis of the study assumed that the wear resistance of the surfaces of hardened parts would be affected not only by their hardness but also by the minimization of internal stresses in the applied layer. It is the minimization of these stresses that will make it possible to obtain the minimum number of cracks in the applied layer and will also ensure its maximum adhesion to the base material.

4. 2. Equipment and materials

For electric spark alloying, industrial equipment "Elitron-24A" [11] was used (Fig. 1, 2), which at a productivity of 0.3...10 cm^2/min makes it possible to obtain a strengthened layer with a thickness of 0.25...2 mm.

The principle of operation is based on the periodic charging of storage capacitors through a transistor switch to a voltage that is set using a set of resistors that determine the processing mode. Then they are discharged through a discharge transistor when the vibrating electrode touches the processing surface.

When the storage capacitors are discharged through the electrode–tool to the electrode–workpiece, the material is transferred from the electrode–tool and dehydrated to the surface of the processed part.

The general view of the equipment is shown in Fig. 1. The installation is equipped with three modules of electrical energy storage, which made it possible to implement different modes of electric spark machining. The power supply was carried out from the AC network with a frequency of 50 Hz at a voltage of 220 V ± 10%. The power consumption of the unit was 0.6 kW. The average productivity of forming a hardened layer on the surface was 5 mm^2/s, and its thickness was 50 μm. The arithmetic mean deviation of the profile did not exceed 20 μm, which ensured high quality of the treated surface (class 5–6). The parameters of the mode used determined the intensity of hardening and the quality of the deposited surface. An increase in power intensified each discharge and, as a result, the transfer of particles from the electrode to the surface of the workpiece.

Fig. 1. General view of the "Elitron-24A" equipment: 1 – vibrator; 2–4 – storage devices; 5 – power supply)

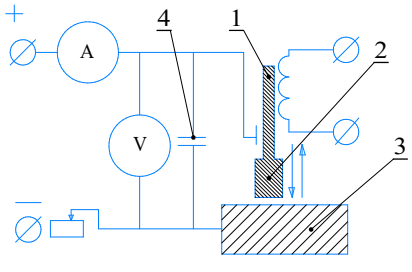

Fig. 2. Schematic diagram of the electric spark installation "Elitron-24A": 1 – vibrator; 2 – electrode (anode); 3 – part (cathode); 4 – capacitor bank

To obtain a uniform coating on a "shaft" type part (pump rod), it was fixed in the cams, and the vibrator was installed on the support of a 16K20 lathe (Fig. 3).

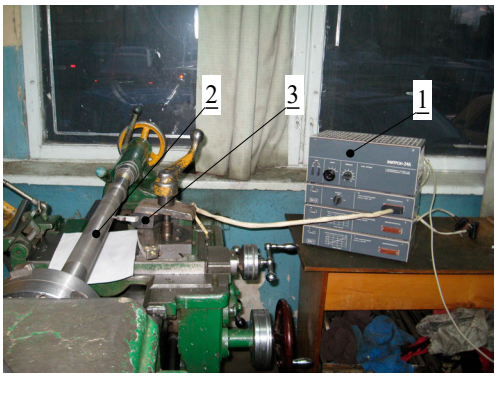

Fig. 3. Bench for electric spark coating: 1 – Electric spark build-up unit "Elitron-24A"; 2 – pump rod; 3 – vibrator mounted on the support of a 16K20 lathe

As electrodes for electric spark build-up and strengthening of the pump rod made of steel 40X (37Cr4KD EN 119), hard

alloy inserts T15K6 (HS123 DIN) and VK8 (HG30, HG40 DIN) were used. The chemical composition of the material of hard alloy electrodes for electric spark doping is as follows: T15K6 – carbides: WC = 79%; TiC = 15%; Co ≤ 6%. VK8 – carbide: WC = 92%; Co ≤ 8%. Chemical composition of the material of the part to be coated: C = 0.36–0.44%; Si = 0.17–0.37; Mn = 0.5–0.8; Ni ≤ 0.3%; S ≤ 0.035%, P ≤ 0.035; Cr = 0.8–1.1%; Cu ≤ 0.3%.

The sample surface was grown in 4 passes using different discharge powers. The growth mode parameters are given in Table 1.

Table 1

Materials and surface build-up modes

Regime	Electrode	Storage capacity, μF	Amplitude of voltage pulses, V	Tool oscillation frequency, Hz	The energy of one pulse, J
T1	T15kK6	60 ± 8	75 ± 15	390 ± 70	0.22
T2		150 ± 15	75 ± 16	250 ± 50	0.42
T3		300 ± 30	71 ± 15	125 ± 25	0.75
B1	VK8	60 ± 8	75 ± 15	390 ± 70	0.22
B2		150 ± 15	75 ± 16	250 ± 50	0.42
B3		300 ± 30	71 ± 15	125 ± 25	0.75

The integration indicator is the energy of one pulse [11]

$$W_p = \frac{1}{2}CU^2. \quad (1),$$

where C is the capacity of the accumulator (capacitor battery), μF;

U – amplitude of voltage pulses, V.

The energy of a single pulse makes it possible to link such characteristics of the installation as the capacity of the capacitor battery and the discharge voltage.

4. 3. Metallographic studies of the deposited layer

After applying the surface layer, blanks were cut from the hardened rods, from which micro sections were made according to [12].

Since a rather thin deposited layer is obtained in the process of electric spark alloying, for its further study and metallographic analysis it is necessary to make an oblique micro section. The design of a sample holder was proposed, which makes it possible to obtain such a micro section in the case of a cylindrical side surface of the part (Fig. 4).

Fig. 4. Specimen holder for making a micro section

For etching the structure, a 3% alcoholic solution of HNO_3 was used.

The structure was analyzed on a scanning electron EVO-40XVP, ZEISS, with a microanalysis system INCA Energy 350, Oxford (Fig. 5). An elemental analysis of the deposited layer was performed [12].

Fig. 5. Scanning electron microscope EVO-40XVP, ZEISS, with microanalysis system INCA Energy 350, Oxford. General view

Basic specifications:

1. Company: Carl Zeiss AG.
2. Categories – Microscopy: Electron: SEM.
3. Features:
– Resolution:
– 3.0 nm at 30 kV (SE and W);
– 2.0 nm at 30 kV (SE and LaB6)/
4. Acceleration voltage: 0.2 to 30 kV.
5. Magnification: 7 to 1,000,000x.
6. Field of view: 6 mm at analytical working distance (AWD).
7. X-ray analysis: 8.5 mm AWD and 35° sweep angle.
8. OptiBeam® modes: Resolution, Depth, Analysis, Wide Field.
9. Available detectors:
– SE in high voltage mode – Everhart –Thornley;
– BSD in all modes – quadrant semiconductor diode;
10. Chamber: 310 mm (Ø) × 220 mm (h)
11. 5-axis motorized sample stage:
– X = 80 mm;
– Y = 80 mm;
– Z = 35 mm;
– T = 0° – 90°;
– R = 360° continuous).
12. Scene control via mouse or joystick and control panel.
13. Image processing:
– resolution: up to 3072 × 2304 pixels;
– signal acquisition by integration and averaging;
– image display: one flicker-free XVGA monitor displaying SEM image at 1024 × 768 pixels.
14. SmartSEM™** system control.
15. Graphical user interface with mouse and keyboard control.
16. Multilingual concise graphical user interface
17. Operating system: Windows® XP.
18. Auxiliary device requirements: 100–240 V, 50 or 60 Hz, single-phase power supply, no water cooling required.

The Vickers microhardness was determined using a PMT-3 device under a load of 200 g as the average value of 10–15 measurements [12].

Basic specifications:

1. Microscope magnification: 130 and 487x.

2. Diamond pyramid:

– angle at the apex: 136°;

– tip at the apex: no more than 1 μ;

– load limits: 2–200 g.

3. Measurement limits of diagonals: impressions (with objective $F = 6.2$): 0.05–0.25 mm.

4. Stage:

– rotation angle limits: ~0–180°;

– longitudinal movement limits: 0–10 mm;

– transverse movement limits: 0–10 mm;

– micrometric feed scale division value: 0.01 mm.

5. Relative effective aperture: illuminator collector: 1:0.7.

6. Power supply: via transformer from AC network 127/220 V.

7. Overall dimensions:

– microhardness tester in working position: 410 × 290 × 200 mm;

– transformer 145 × 110 × 70 mm.

8. Weight:

– microhardness tester: 21.6 kg;

– transformer: 1.72 kg.

The method is based on the process of smooth indentation of a tetrahedral diamond pyramid with an apex angle of 136°. The main parameter for measurement is the diagonal of the impression formed on the surface of the sample. The hardness value is determined by the ratio of the applied load P to the area of the impression surface

$$HV = \frac{P}{A} = 0.1891\left(\frac{F}{d^2}\right) \text{GPa}, \quad (2)$$

where P is the applied force, N;

d is the diagonal of the imprint, m.

4. 4. Determining residual stresses in the applied layer

To determine the internal stresses in the coating, we used a scheme in which the surface layer is applied to a freely unclamped plate and the equilibrium shape of which is established during the application of this layer. Residual stresses are calculated from the following formula [12]:

$$\sigma_{\max} = [E \cdot h_1 \cdot (h_1 - h_2)] / 6 \cdot \rho_k \cdot h_2, \quad (3)$$

$$\rho_k = L^2 / 8 \cdot \delta_{\max}, \quad (4)$$

where $\sigma_{\max}$ – maximum internal stresses in the surface layer;

E – modulus of elasticity of the plate material;

L – plate length;

h_1 – plate thickness;

h_2 – thickness of the built-up layer;

ρ_k – radius of curvature of the plate;

$\delta_{\max}$ – maximum deflection of the plate.

4. 5. Tribological studies

To study the wear resistance of surfaces hardened by electric spark alloying, it is proposed to use a universal friction machine model 2168 UMT (Fig. 6).

To reproduce the wear process of hardened working surfaces as accurately as possible, a reciprocating motion test scheme was chosen, which is implemented by installing an additional device – a chamber, which is part of the machine. The principle of operation is as follows: the electric motor rotates the spindle, on which the worm gear is installed, and drives crank 1 through the worm wheel shaft, which is connected to the test rod according to the kinematic diagram shown in Fig. 7. Crank 1 drives connecting rod 2, which in turn is connected to the fork (eye) of the slider, on which the movable sample, rod 5, is fixed. Two fixed samples, fingers 4, are pressed against rod 3, which are placed in chamber 5.

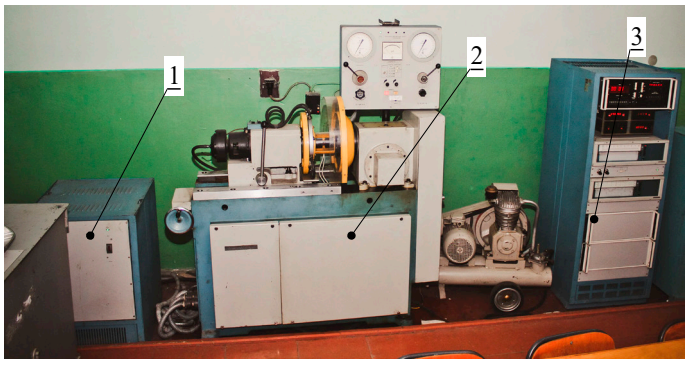

Fig. 6. General view of the friction machine 2168 UMT: 1 – power unit; 2 – friction machine; 3 – control panel

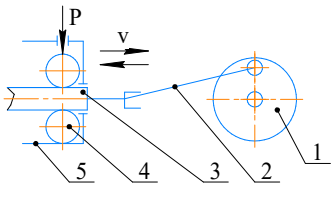

Fig. 7. Kinematic diagram of the rod-finger test: 1 – crank; 2 – connecting rod; 3 – moving sample; 4 – stationary sample; 5 – chamber

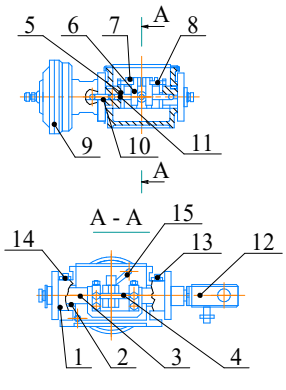

Fig. 8. Schematic of a reciprocating test chamber for samples: 1 – collapsible housing; 2 – bearings; 3 – slider; 4 – sample rod; 5 – housing; 6 – sample finger; 7 – clamp; 8 – bolt; 9 – pneumatic chamber; 10 – rod; 11 – rod; 12 – fork; 13 – fitting; 14 – fitting; 15 – tube

The test chamber (Fig. 8) consists of collapsible housing 1. In bearings 2 of the housing, slider 3 moves with the sample, rod 4 (Fig. 8), which is attached to the slider with screws. Perpendicular to the sample rod, housing 5 with two sample fingers 6 (Fig. 8) is installed. Before installation in the hous-

ing, clamps 7 are installed on the fingers and secured with bolts 8. The fingers of the sample are pressed against the rod by the force created by pneumatic chamber 9 through rods 10 and 11. The slider moves in the housing bearings using the eye (fork) 12.

To cool the bearings, coolers are installed on them, which can be connected to a collector mounted on the frame. The bearings are lubricated through fittings 13 and 14, and the medium (liquid) in which the friction pair is tested is supplied through tube 15 fixed to the chamber housing. The general structure of this reciprocating test chamber is shown in Fig. 9.

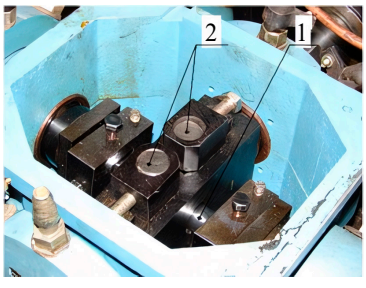

Fig. 9. Reciprocating test chamber for testing samples:
1 — sample rod; 2 — sample fingers

Existing methods of testing materials for wear do not allow for sufficiently accurate modeling of the wear process of steel counter-samples when interacting with elastically fixed abrasive grains. Such interaction occurs during the contact of the pump rods with the seal. In addition, there are difficulties in terms of uniform distribution of the applied force along the entire length of the elastic sample, as well as periodic introduction of the unworn part of the elastic sample into contact with the metal sample.

Therefore, the method of testing materials for wear has been improved by increasing the friction coefficient by introducing a sample of abrasive grains into the elastic material, which would allow the modeling conditions to be closer to the wear conditions of actual parts.

The task is solved by adding an abrasive material, quartz sand, to raw (unvulcanized) rubber. The resulting mass is mixed and vulcanized, after which the formed sample is installed in a sample holder made in the form of a truncated sleeve (Fig. 10). The rubber sample is periodically moved in the axial direction, introducing the unworn part of the stationary sample into the contact zone of the moving metal countersample.

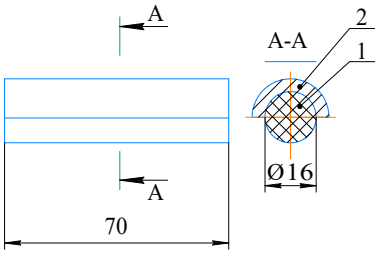

Fig. 10. Elastic stationary specimen for wear testing:
1 — elastic counterbody; 2 — specimen holder

The moving specimen for wear tests is made of the same material as the pump rod (steel 40X) (Fig. 11). The coating is applied under the same modes as on the original part. This approach will allow the most accurate simulation of the pump rod operation.

To get a continuous coating, it is obtained using a lathe (Fig. 3). Machine operating modes: spindle speed, $n = 0.75$ s^{-1}; feed rate, $s = 0.455$ mm/rev.

Fig. 11. Movable steel finger for wear testing

Specific loads on the samples are created using pneumatic chamber 9 (Fig. 8). The force on the rod of the pneumatic chamber is selected by trial and error to provide a specific contact pressure equal to 1.2 MPa. To this end, we alternately create increasing forces on the rod of the pneumatic chamber, simultaneously determining the contact area of the elastic and rigid counter-samples using a copier. By trial and error, we stop at a force of 725 N, at which the contact area is 3 cm^2. Since there is simultaneous contact with two elastic counter-samples, the total friction area is 6 cm^2.

The duration of each test cycle of the sample is selected depending on the predicted wear resistance of the friction surface.

The friction path is determined from the following formula

$$L_r = 2n_x \cdot l_x \cdot t_r, \text{m}, \quad (5)$$

where n_x is the frequency of double strokes, strokes/min;

l_x is the stroke length, m, $l_x = 12$ mm;

t_r is the cycle time, min.

5. Results of investigating the influence of processing modes on the operational characteristics of the surface layer

5. 1. Results of metallographic studies

A typical structure of the layer grown on the surface of the rod obtained using hard alloys VK8 and T15K6 as an anode is shown in Fig. 11. The thickness of the grown layer on the surface of the rod (light strip in Fig. 11) ranged from 8 to 20 μm during the implementation of the modes given in Table 1. This layer is practically not subject to etching, which indicates a significant concentration of alloying elements.

The microhardness of the obtained layer varied depending on the processing mode used from 10 to 15.2 GPa (Table 2). The maximum microhardness (~15.2 GPa) was recorded when implementing the T2 mode using the T15K6 hard alloy electrode. The microhardness of the deposited

layer using the same electrode, but using other deposition modes, does not exceed 11 GPa. The average microhardness of the deposited layer when using the VK8 electrode for processing does not exceed 11...14 GPa. The microhardness is highest when using the B3 mode (Table 1).

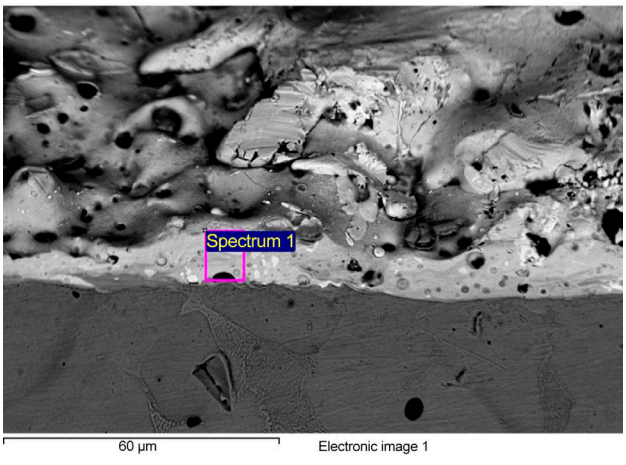

a

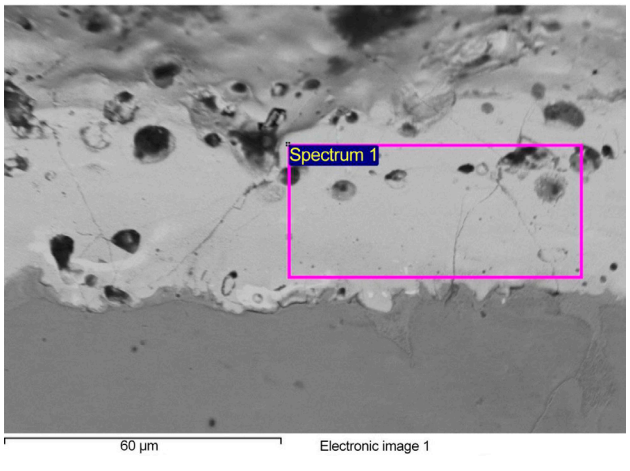

b

Fig. 12. Typical microstructures of the hardened surface layer of a pump rod made of 40X steel: *a* – obtained using BK8 hard alloys as an anode; *b* – T15K6 as an anode

Table 2

Elemental composition of the surface layer of 40X steel, hardened by different ESA regimes with T15K6 and VK8 hard alloys (results of spectral microanalysis of the surfaces of hardened layers with an area of ~500 μm^2)

ESA regime	Content of elements in the hardened layer, wt %					
	W	Co	Ti	Fe	O	C
T1	27.2	2.1	4.3	48.4	9.7	8.3
T2	57.4	4.1	9.8	10.2	5.5	13.0
T3	67.8	5.2	9.4	9.0	–	8.6
B1	55.5	–	–	31.1	2.3	11.1
B3	54.5	4.2	–	17.9	6.6	16.8

The microhardness of the base metal (40X steel) directly under the deposited layer was 1600...1900 MPa, which is typical for ferrite as a component of steels with a ferritic-pearlitic structure.

The elemental composition of the deposited layer is given in Table 2. Mechanical characteristics are given in Table 3.

Table 3

Characteristics of layers surfaced by electric spark treatment

Regime	Electrode	Average thickness of the surfaced layer, μm	Microhardness HV, GPa, ± 5%
T1	T15K6	10	10.2
T2		15	15.2
T3		15	10.5
B1	BK8	10	11.5
B2		20	11.6
B3		20	13.5

Thus, data were obtained that illustrate the influence of the technological parameters of ESA on the properties of the treated surfaces.

5. 2. The magnitude of residual stresses in the deposited layer

The dependence of residual stresses on the processing parameters is given in Table 4.

Table 4

Characteristics of layers surfaced by electric spark treatment

Regime	Electrode	Residual stresses, MPa
T1	T15K6	1340
T2		710
T3		900
B1	BK8	900
B2		900
B3		–90

Under mode B3, we obtain a small modulus of compressive stress, which helps minimize the number of cracks.

5. 3. Results of tribological studies

Fig. 13, 14 show the dependence of weight wear on the friction path.

Minimum weight wear is characteristic of modes B3 and T2.

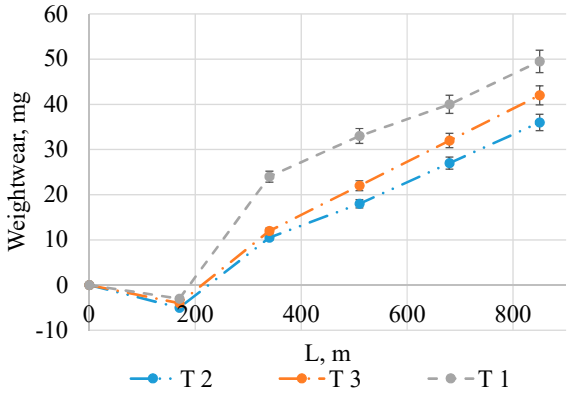

Fig. 13. Dependence of weight wear of 40X steel with ESA T15K6 coating applied under T1, T2, T3 modes (Table 2) on friction trajectory L (specific pressure 1.2 MPa, speed 120 rpm)

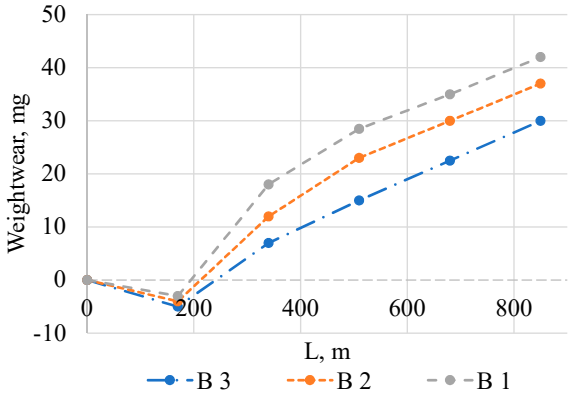

Fig. 14. Dependence of weight wear of 40X steel with ESA VK8 coating applied under modes B1, B2, B3 (Table 2) on friction trajectory L (specific pressure 1.2 MPa, speed 120 strokes/min)

6. Discussion of results of investigating the influence of processing modes on the operational characteristics of surface layer

Analysis of the microstructure of the surface layers of 40X steel, hardened by ESA technology using electrodes made of T15K6 and VK8 hard alloys, revealed that microcracks spread to their entire depth after all ESA modes (Fig. 12).

As a rule, cracks are oriented at an angle of ~45° to the hardened surface, which could be a consequence of facilitated shear. They could be caused by high residual stresses in the hardened layer, which were able to relax due to the appearance of such cracks. The highest microhardness of the hardened layer was obtained after ESA using the T2 mode (Fig. 12), under which its greatest depth (up to 15 μm) was reached (Fig. 12, *b*).

Analysis of the elemental composition of the surface layers strengthened by T15K6 carbide plates revealed that after ESA under the T1 regime, the layer contains almost half as many carbide-forming elements (W, Ti) as under the T2 and T3 regimes (Table 2). After all, it is carbides of the TiC, WC, W^2C type that ensure its hardness after ESA. Cobalt from the hard alloy electrode acts as a high-strength filler-bond for carbides and, as spectral analysis shows, is fairly evenly distributed throughout the thickness of the strengthened layers. At the same time, Fe, Ti, and W are distributed unevenly (the maxima in the Fe distribution correspond to the minima in the Ti and W distributions). One of the lowest values of the microhardness of the surface layer treated under the T1 regime is caused by the highest Fe content in it (Table 2). And the surface microhardness after the T3 regime (with the maximum amount of W, Ti, and Co) is the lowest (possibly due to insufficient carbon concentration for carbide formation). After all, after the T2 regime, when the microhardness of the hardened layer is maximum, the carbon content in it is significantly higher. Our results on the use of ESA technology for the restoration of worn elements are consistent with the literature data, for example [13–20].

The authors of [13] note that to ensure the operability of surface-hardened elements under difficult operating conditions, it is necessary to obtain a sufficiently high microhardness of the surface layer.

In works [14, 15], the tribological characteristics of metal-polymer friction pairs operating in brake assemblies were studied under production and laboratory conditions. The dependences of the dynamic friction coefficient on circulating tribocurrents and the degree of linear wear of friction pairs in brake assemblies on tribocurrents generated in the contact zone of two-layer metal-polymer structures were also studied.

The authors of [16] studied the dependences of the dynamic friction coefficient on circulating tribocurrents and the degree of linear wear of friction pairs in brake assemblies on tribocurrents generated in the contact zone of two-layer metal-polymer structures. Despite a fundamentally different explanation of the physics of the process, they came to the conclusion that the wear resistance of coatings is affected not only by the hardness of the contacting surfaces but also by other factors.

The authors of paper [17] investigated the formation of the structure and wear resistance to impact abrasion of the deposited layers applied by arc welding with flux-cored wires of high-manganese austenitic steel. The method of strengthening surfaces proposed by them, despite its progressiveness, is much more expensive and technologically more complex.

Work [18] confirms the idea that electric spark alloying has already been recognized as a cost-effective method for applying surface coatings. Its implementation requires simple and inexpensive equipment. In addition, the mechanical and tribological properties of coatings applied using ESA are very promising. The applied coatings have significantly better tribological properties compared to the properties of the substrate. When the coatings are secondarily treated with a laser beam, they obtain a smoother surface and an amorphous structure.

The authors of [19] claim that low surface roughness after electric spark alloying was achieved by correctly selecting the parameters of the pulses in the group and the pauses between them. This coincides with our vision of the correct selection of the technological parameters for ESA.

Paper [20] described the strengthening methods that increase the wear resistance and corrosion resistance of the working surfaces of machine parts. It was established that among the metal coatings, chromium coatings are most often used.

Thus, the results of determining the influence of technological parameters on the properties of the deposited layer, insufficiently studied in existing works, provide opportunities for their use in the processes of electric spark alloying of hard alloy electrodes.

After ESA under the T2 mode, a finely dispersed eutectic of TiC-WC carbides with a size of 0.05...0.1 μm was found in the structure of the surface layer. Since they are absent in the structure of the surface layers processed under the T1 and T3 regimes, it was with them that the highest microhardness of the layer after the T2 regime was associated. The structure of the surface layers of steel 40X after ESA using electrodes made of hard alloys VK8 and T15K6 was visually almost indistinguishable (Fig. 12). However, their microhardness changed significantly. In particular, the similarity of microstructures in layers with maximum microhardness obtained using alloys T15K6 (under the T2 regime) and VK8 (under the B3 regime) is obvious. In both cases, round pits were found on the surfaces of oblique cuts, at the bottom of which there were mostly oxide inclusions. The largest in size were the pits after the B2 regime, and the smallest number of them was found after the B1 regime. After the B3 regime, a significant amount of fine oxides was observed, which is due to the integrally high oxygen content in the surface layer.

The tungsten content in the surface layers hardened by electrodes made of VK8 alloy practically does not depend on the

processing mode (Table 2). After the B1 mode, the highest iron content was recorded there, and cobalt was not identified at all. This explained the lowest microhardness of the layer hardened by the B1 mode. Since the carbon content in the layer after the B3 mode is higher than after the B1 mode, the slightly higher microhardness was associated with more favorable prerequisites for the formation of a larger number of tungsten carbides. It was established that when using electrodes made of T15K6 hard alloy, tensile stresses of the first kind appear in the surface layer under all hardening modes, which during ESA depend on the heating temperature, cooling rate, reduction in metal volume during crystallization, and the tendency of the hardened layer to relax them due to the formation of a network of microcracks in it. In particular, at maximum tensile stresses (after the T1 regime), minimal cracking of the hardened layers was observed, and at significantly lower ones (after the T3 regime), maximal cracking was observed. The optimal combination of microhardness and residual stresses after the T2 regime with the average values of the energy of a single pulse and the frequency of electrode vibration was (Table 1). When using an electrode made of VK8 alloy, tensile stresses in the hardened layer arose only under regimes B1 and B2, and under regime B3, compressive stresses. Cracks in the layer hardened under regime B3 were practically not found, which could be a consequence of the occurrence of compressive residual stresses in it. In addition, under this regime, mixing of the molten metal in the zones of electric spark flashes on the substrate was minimal due to the lowest frequency of electrode vibration (Table 1). This contributed to the appearance of a significant amount of WC carbides in the hardened layer and, as a result, provided it with the maximum (among those obtained using VK8 electrodes) microhardness.

Three factors influencing the operability of surface-hardened structural elements under harsh operating conditions have been identified. First, the electric spark alloying technolgy should ensure high microhardness of the surface layer due to its saturation with carbide-forming elements. Second, the size and density of oxides in the hardened layer should be optimal because they determine its porosity and the ability of the matrix to relax residual stresses. Third, minimizing tensile residual stresses in it, which are responsible for cracking of the hardened layer. Optimization of the influence of all these factors is a necessary prerequisite for using this method of surface strengthening to restore worn surfaces of parts.

However, the proposed methodology has a number of limitations. In particular, this concerns the fact that the use of various materials as electrodes requires a large amount of research to determine the operational parameters of the applied layer. A further development of the study could be the construction of a mathematical model that would take into account the influence of magnitude of the initial factors on the result.

7. Conclusion

1. Based on our results of a comprehensive study of the structure, microhardness, and content of carbide-forming elements in the hardened layers on the surface of 40X steel obtained by different modes of electric spark alloying with T15K6 and VK8 hard alloys, the technological parameters of surface hardening with tungsten carbide to a depth of 15 and 20 μm have been optimized. At a single pulse energy of 0.42 and 0.75 J, as well as an electrode vibration frequency of 250 ± 50 and 125 ± 25 Hz, the microhardness of the hardened layer formed by electrodes made of T15K6 and VK8 hard alloys was 15.2 and 13.5 GPa.

2. The magnitude of residual stresses in the applied coatings has been determined. The residual stresses in the strengthened layer formed by the T15K6 hard alloy electrode at a unit pulse energy of 0.22 and an electrode vibration frequency of 390±70 are 1340 MPa. The residual stresses in the strengthened layer formed by the VK8 hard alloy electrode at a unit pulse energy of 0.75 J and an electrode vibration frequency of 125 ± 25 Hz are 90 MPa, respectively. It is under these modes that the maximum and minimum number of microcracks in the applied coatings are observed (Fig. 12).

3. When using T15K6 as electrodes, the lowest weight wear during the passage of 850 m of the friction path is observed under the T2 mode (0.036 g, hardness 15.2 GPa, residual tensile stresses 710 MPa). When using VK8 as electrodes, the lowest weight wear during the passage of 850 m of the friction path is observed under the B3 mode (0.03 g, hardness 13.5 GPa, residual compressive stresses 90 MPa). The sample hardened under the B3 mode has better wear resistance than the sample hardened under the T2 mode, although it is inferior to the latter in microhardness. This is explained by the better quality of the applied layer (minimum residual stresses and, as a result, a minimum of microcracks).

Conflicts of interest

The authors declare that they have no conflicts of interest in relation to the current study, including financial, personal, authorship, or any other, that could affect the study, as well as the results reported in this paper.

Funding

The research was funded as part of the implementation of research work under state registration number RK 0124U003990.

Data availability

All data are available, either in numerical or graphical form, in the main text of the manuscript.

Use of artificial intelligence

The authors confirm that they did not use artificial intelligence technologies when creating the current work.

References

1. Tarelnyk, V., Konoplianchenko, I., Tarelnyk, N., Kozachenko, A. (2019). Modeling Technological Parameters for Producing Combined Electrospark Deposition Coatings. Materials Science Forum, 968, 131–142. https://doi.org/10.4028/www.scientific.net/msf.968.131
2. Katinas, E., Jankauskas, V., Kazak, N., Michailov, V. (2019). Improving Abrasive Wear Resistance for Steel Hardox 400 by Electro-Spark Deposition. Journal of Friction and Wear, 40 (1), 100–106. https://doi.org/10.3103/s1068366619010070

3. Lu, K., Zhu, J., Ge, W., Hui, X. (2022). Progress on New Preparation Methods, Microstructures, and Protective Properties of High-Entropy Alloy Coatings. Coatings, 12 (10), 1472. https://doi.org/10.3390/coatings12101472
4. Zhengchuan, Z., Guanjun, L., Konoplianchenko, I., Tarelnyk, V. B., Zhiqin, G., Xin, D. (2022). A review of the electro-spark deposition technology. Bulletin of Sumy National Agrarian University. The Series: Mechanization and Automation of Production Processes, 2 (44), 45–53. https://doi.org/10.32845/msnau.2021.2.10
5. Wang, J., Zhang, M., Dai, S., Zhu, L. (2023). Research Progress in Electrospark Deposition Coatings on Titanium Alloy Surfaces: A Short Review. Coatings, 13 (8), 1473. https://doi.org/10.3390/coatings13081473
6. Leo, P., Renna, G., Casalino, G. (2017). Study of the Direct Metal Deposition of AA2024 by ElectroSpark for Coating and Reparation Scopes. Applied Sciences, 7 (9), 945. https://doi.org/10.3390/app7090945
7. Cao, G., Zhang, X., Tang, G., Ma, X. (2019). Microstructure and Corrosion Behavior of Cr Coating on M50 Steel Fabricated by Electrospark Deposition. Journal of Materials Engineering and Performance, 28 (7), 4086–4094. https://doi.org/10.1007/s11665-019-04148-2
8. Salmaliyan, M., Malek Ghaeni, F., Ebrahimnia, M. (2017). Effect of electro spark deposition process parameters on WC-Co coating on H13 steel. Surface and Coatings Technology, 321, 81–89. https://doi.org/10.1016/j.surfcoat.2017.04.040
9. Jiao, Z., Peterkin, S., Felix, L., Liang, R., Oliveira, J. P., Schell, N. et al. (2018). Surface Modification of 304 Stainless Steel by Electro-Spark Deposition. Journal of Materials Engineering and Performance, 27 (9), 4799–4809. https://doi.org/10.1007/s11665-018-3579-0
10. Tarelnyk, V., Martsynkovskyy, V., Gaponova, O., Konoplianchenko, I., Dovzyk, M., Tarelnyk, N., Gorovoy, S. (2017). New sulphiding method for steel and cast iron parts. IOP Conference Series: Materials Science and Engineering, 233, 012049. https://doi.org/10.1088/1757-899x/233/1/012049
11. Kozak, F. V., Prunko, I. B., Fedenko, V. Y., Gladun, M. R. (2024). Optimization of the process of application of electrospark coatings when strengthening automotive parts of the “shaft” type. Oil and Gas Power Engineering, 2 (40), 66–72. https://doi.org/10.31471/1993-9868-2023-2(40)-66-72
12. Kryshtopa, S., Kryshtopa, L., Bogatchuk, I., Prunko, I., Melnyk, V. (2017). Examining the effect of triboelectric phenomena on wear-friction properties of metal-polymeric frictional couples. Eastern-European Journal of Enterprise Technologies, 1 (5 (85)), 40–45. https://doi.org/10.15587/1729-4061.2017.91615
13. Kryshtopa, S. I., Petryna, D. Yu., Bogatchuk, I. M., Prun’ko, I. B., Mel’nyk, V. M. (2017). Surface Hardening of 40KH Steel by Electric-Spark Alloying. Materials Science, 53 (3), 351–358. https://doi.org/10.1007/s11003-017-0082-y
14. Kryshtopa, S., Kozhevnykov, A., Panchuk, M., Kryshtopa, L. (2018). Influence of triboelectric processes on friction characteristics of brake units of technological transport. Naukovyi Visnyk Natsionalnoho Hirnychoho Universytetu, 3, 87–93. https://doi.org/10.29202/nvngu/2018-3/10
15. Kryshtopa, S. I., Prun’ko, I. B., Dolishnii, B. V., Panchuk, M. V., Bogatchuk, I. M., Mel’nyk, V. M. (2019). Regularities of Wear of Metal-Polymer Friction Couples Under the Influence of Tribocurrents. Materials Science, 55 (2), 193–200. https://doi.org/10.1007/s11003-019-00288-x
16. Hvozdets’kyi, V. M., Sirak, Ya. Ya., Zadorozhna, Kh. R., Dem’yanchuk, Ya. M. (2018). Influence of the Size of Drops and the Velocity of Flow on the Structure and Properties of Electric-Arc Coatings. Materials Science, 53 (5), 702–708. https://doi.org/10.1007/s11003-018-0126-y
17. Prysyazhnyuk, P., Ivanov, O., Matvienkiv, O., Marynenko, S., Korol, O., Koval, I. (2022). Impact and abrasion wear resistance of the hardfacings based on high-manganese steel reinforced with multicomponent carbides of Ti-Nb-Mo-V-C system. Procedia Structural Integrity, 36, 130–136. https://doi.org/10.1016/j.prostr.2022.01.014
18. Rukanskis, M. (2019). Control of Metal Surface Mechanical and Tribological Characteristics Using Cost Effective Electro-Spark Deposition. Surface Engineering and Applied Electrochemistry, 55 (5), 607–619. https://doi.org/10.3103/s1068375519050107
19. Ribalko, A. V., Sahin, O., Korkmaz, K. (2009). A modified electrospark alloying method for low surface roughness. Surface and Coatings Technology, 203 (23), 3509–3515. https://doi.org/10.1016/j.surfcoat.2009.05.002
20. Bembenek, M., Kopei, V., Ropyak, L., Levchuk, K. (2023). Stressed State of Chrome Parts During Diamond Burnishing. Metallofizika I Noveishie Tekhnologii, 45 (2), 239–250. https://doi.org/10.15407/mfint.45.02.0239